Sustainable Structures
ISSN: 2789-3111 (Print); ISSN: 2789-312X (Online)
http://www.sustain-dpl.com/journal/sust
DOI: 10.54113/j.sust.2023.000032

*ORIGINAL ARTICLE*

# Deformation and energy dissipation of steel box girders of cable-stayed bridges subjected to blast loadings

**Yu Zhu [a], Shaoyu Zhao [b], Yuye Zhang [c,*]**

[a] Department of Civil Engineering, Nanjing University of Science and Technology, Nanjing 210094, China.
[b] School of Engineering, RMIT University, Bundoora, VIC 3083 Australia.
[c] Department of Civil Engineering, Nanjing University of Science and Technology, Nanjing 210094, China.
[*] Correspondence: zyy@njust.edu.cn; Tel.: +86-025-84315773.

**Abstract: S**teel box girders are widely used in cable-stayed bridges, while they are prone to severe damage under explosions. This paper investigates the deformation and energy dissipation of steel box girder of cable-stayed bridges under blast impact, caused by the accidental explosions of tanker trucks and vehicles. In this study, Hypermesh and LS-DYNA are employed to simulate the dynamic responses of a real steel box girder cable-stayed bridge under explosions. The deformation response and energy absorption of the box girder under explosions are investigated. Several failure modes and failure processes are analyzed and summarized. The findings indicate that the failure mode of an orthotropic steel bridge panel under blast impact is primarily local damage, with the damage process being divided into three stages: local plate deformation, fragment formation, and petal formation. For bridge deck explosions, the main energy dissipation components of steel girders are the bridge panel, web, diaphragm and rib stiffeners. The research results can provide the basis for the follow-up study on the anti-explosion safety of bridge structures.

**Keywords:** Cable-stayed bridge, steel box girder, deformation response, energy dissipation, explosion load

## 1 Introduction

In recent years, the damage and destruction of bridge structures under various explosions have occurred from time to time, caused by the accidental explosions of tanker trucks and vehicles or intentional explosions. However, the existing design guidelines for blast proof bridges are limited to specific structural members, and little attention has been paid to the responses of civil bridge structures under blast impact [1-2]. Thus, it is necessary to investigate the local and overall performance of bridge members (deck, pier, tower) under different air explosion pressures at different locations and intensities.

Bridge structures are generally more susceptible to extreme loads than buildings because they have less structural redundancy compared to buildings [3-5]. Therefore, in the case of failure of any major component in a bridge, it is almost impossible to redistribute the applied load through different load paths to prevent potential progressive collapse. Similarly, when a large explosion occurs above the bridge deck, serious damage to the bridge deck may also lead to cable anchorage loss, and further lead to the gradual collapse and loss of the entire bridge [6-8]. A large number of dangerous goods, flammable and explosive goods transport vehicle accidents are one of the main reasons for the



Received: 18 April 2023; Received in revised form: 5 September 2023; Accepted: 2 October 2023

explosions [9]. In addition, the remaining bearing capacity of the support unit is crucial to the overall stability and the safety of the occupants [10]. The assembly joint of steel box is usually regarded as one of most important components in the structures. Furthermore, the violence of some phenomena such as tornadoes and thunderstorms can aggravate the already compromised quality of these materials, favoring the detachment of the surface layers to the point of compromising the safety of some structure and infrastructures [11]. Exposed to extreme external loads (such as shock, explosion and fire), the steel components will be permanently deformed or completely destroyed, potentially leading to catastrophic accidents [12-13]. As an important transportation hub, once the bridge is damaged by explosion, it is easy to cause serious economic loss and social impact [14]. In order to avoid such serious consequences, the mechanical behavior and dynamic response of bridges should be intensively studied. The numerical simulation method has been widely used in the study of the impact of explosion on structure, and reliable results of structural response prediction have been obtained [15]. In addition, Zhu [16] proposed a simplified method and the corresponding indexes suitable for antiknock design of long-span cable-bearing bridges.

For the study on the local anti-explosion of Bridges, Ibrahim et al. [17] analyzed the dynamic response of single-span simply supported prestressed concrete box girder under the blast wave action of seven kinds of explosives with different equivalents (the detonation center is 0.762m away from the bridge panel) by using LS-DYNA. Wei et al. [18] carried out the comparative study on the lateral displacement and failure of the square section of prestressed concrete column situation using the same numerical method for different scale distances under the action of the explosion. Shi [19] analyzed the dynamic response, failure mode and key factors affecting the anti-explosion performance of prestressed concrete columns under explosion loads, and established a pressure-impulse damage assessment method based on residual bearing capacity. Yao [20] studied the dynamic response of single-deck steel box girder bridge attacked by terrorist explosion, and he focused on analyzing the local damage mechanism of steel box girder under the blast effect of typical bags and car bombs. Yu [21] used AUTODYN to analyze the dynamic response and failure mode of reinforced concrete cylindrical pier under underwater explosion, carried out parameter analysis (proportional distance, reinforcement ratio, hoop ratio, etc.), and also discussed the anti-explosion performance of reinforced concrete cylindrical pier with isolation steel plate and steel cylinder.

As for the overall anti-explosion of a bridge, Deng et al. [22] considered the coupling effect of explosives, air and bridge, in which the explosion location was 1.25 m away from the main span bridge deck. They applied the nonlinear dynamic finite element method to carry out a three-dimensional numerical analysis of the damage of a continuous steel truss cable-stayed bridge with single tower and double cable plane under the action of explosion shock wave. Tang et al. [23] used ATBLAST to calculate the explosion load. LS-DYNA was used to analyze the dynamic response and failure of a long-span cable-stayed bridge (main span is steel-mixed box girder, back span is reinforced concrete box girder) under the explosion action at different locations (0.5m from the ground of bridge pier and tower, 1.0m above the bridge floor). On the basis of the overall bridge collapse analysis, the antiknock safety distance of key components is given. Wang [24] used the deflection theory and numerical simulation based on LS-DYNA to analyze the vertical bending response of suspension bridge under the action of shock wave in view of the bomb aerial explosion where the suspension bridge may suffer in wartime. In addition, the influence of different TNT equivalent explosives at different heights and horizontal positions directly above the axis of the bridge on the deformation and internal force of the suspension bridge structure is considered. Chen [25] used LS-DYNA to simulate and analyze the dynamic response and collapse process of continuous rigid frame bridge under explosion load by changing the position and equivalent of explosives, and used Tuler-Butcher damage model to obtain the damage accumulation curve of the specified unit. Yang [26] proposed a safety index based on the maximum cumulative stress of the control section under explosion and its material yield strength to evaluate the safety performance of bridge structure under explosion. LS-DYNA was also used to analyze and evaluate the dynamic response and safety performance of a large steel truss composite arch bridge under different explosion loads.

In this paper, the method of Hypermesh combined with LS-DYNA finite element simulation is used to analyze the damage of steel box girders caused by the explosion of car bomb and oil tanker. Firstly, the cable-stayed bridge is modeled in detail, and the gravity is applied to the whole model and

the dynamic relaxation is carried out to make it stable. Secondly, because the damage caused by the explosion is local, the explosion analysis is carried out on the mid-span steel box girder, and the method of complete restart of LS-DYNA is used to impose the initial internal force on the steel box girder. This paper focuses on the analysis of the dynamic response process of steel box girder under the action of explosion load, failure mode, deformation and energy dissipation without breaking, crack development process, deformation energy and fragment kinetic energy when breaking and energy dissipation of different structures. According to the research results of this paper, the main energy dissipation and damage parts of the bridge under the action of explosion load are determined, which provides theoretical support for the future protection work. At the same time, it also provides the basis for the stability analysis of the whole bridge (the stress redistribution of the whole bridge due to the local failure).

## 2 Calculation model of steel box girder

This section mainly describes the model verification and the setting of working conditions. In order to understand the actual behavior of orthotropic bridge deck under explosion load, a typical steel orthotropic bridge deck in long-span cable-stayed bridges is modeled, and the explosion on the bridge deck is simulated. The parameters that vary in the analysis are the explosion equivalent, the location of the explosion, and the high strain rate mechanical properties of the steel material used in the orthotropic deck. Through dynamic analysis, the performance of orthotropic bridge deck under explosion load is discussed, and the failure mode is determined.

### 2.1 Model verification

Zhao et al. [27] designed the box-like specimen as shown in **Fig. 1** to consider the lateral explosion load. In order to study the dynamic response mode and damage characteristics of the stiffened plates under different loading directions, the internal stiffened plates and external stiffened plates were considered in the specimen. The sample is made by fillet welding on both sides of Q235B steel plate (**Fig. 1**). Four groups of working conditions, and explosive yield and specimen size were designed.


(a) Whole specimen (outside) (b) Detail specimen (inside) (c) Whole specimen (inside)

**Fig. 1.** The test specimen designed by Zhao et al [27].

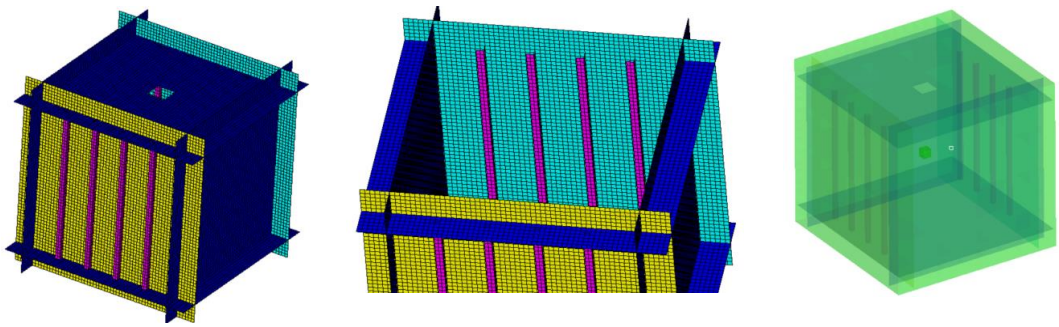

(a) Integral finite element model of steel box (b) Finite element model of steel box interior (c) Finite element model of air and explosives

**Fig. 2.** Finite element model.

Hypermesh is combined with LS-DYNA for simulation. Since only experimental results at normal temperature are simulated, only steel pipe, air and explosive units are established. Steel pipe adopts shell unit, while air and explosive adopt solid unit, as shown in **Fig. 2**.

The maximum deflections under four groups of working conditions are mainly compared to verify the influence of stiffener and explosive equivalent on steel plate. Materials 24 (see **Table 1** for specific parameters), 8 (**Table 2**) and 9 (**Table 3**) are used for steel, explosives and air, respectively. The equation of state for explosives uses EOS2 and air uses EOS1. For detailed parameters, see **Table 1-3**, where $E_0$ and $V_0$ are initial internal energy and initial relative volume per unit reference volume respectively, $A$, $B$, $R_1$ , $R_2$ and $\omega$ are material constants.

**Table 1.** 24 material specific parameters table

| Material identification | Mass density (kg/m$^3$) | Young's modulus (MPa) | Poisson's ratio | Yield stress (MPa) | Failure flag | Strain rate parameter, $C$ | Strain rate parameter, $P$ |
|---|---|---|---|---|---|---|---|
| 24 | 7850 | 2.06e5 | 0.3 | 345 | 0.4 | 40 | 5 |

**Table 2.** 8 material and equation of state parameters table

| Material identification | Mass density (kg/m$^3$) | Detonation velocity (m/s) | Chapman-Jouget pressure (GPa) | A (GPa) | B (GPa) | $R_1$ | $R_2$ | $\omega$ | $E_0$(MJ/m$^3$) |
|---|---|---|---|---|---|---|---|---|---|
| 8 | 1590 | 6930 | 28.6 | 598.155 | 13.75 | 4.5 | 1.5 | 0.32 | 8700 |

**Table 3.** 9 material and equation of state parameters table

| Material identification | Mass density (kg/m$^3$) | $C_0$ | $C_1$ | $C_2$ | $C_3$ | $C_4$ | $C_5$ | $C_6$ | $E_0$(J) | $V_0$ |
|---|---|---|---|---|---|---|---|---|---|---|
| 9 | 1.293 | 0 | 0 | 0 | 0 | 0.4 | 0.4 | 0 | 253312.5 | 1 |

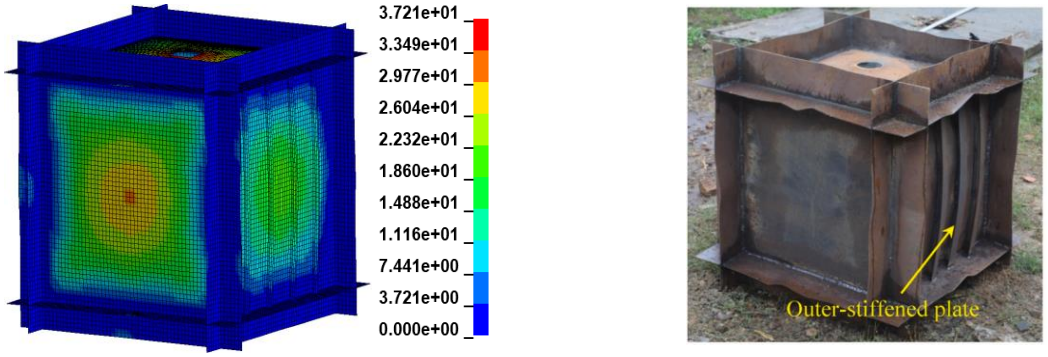


(a) Simulated deformation results under working condition 1 (unit: cm)

(b) Photos of actual results in working condition 1 [27]

**Fig. 3.** Comparison of results.

The comparison between the simulated and experimental deformation results under the four groups of operating conditions is shown in **Table 4** below, which indicates that the simulation results are relatively reliable.

**Table 4.** Comparison between simulated deformation results and experimental deformation results, unit: mm

| Case | Internal stiffeners | | External stiffeners | | No stiffener | |
|---|---|---|---|---|---|---|
| | Simulation result | Experimental result [27] | Simulation result | Experimental result [27] | Simulation result | Experimental result [27] |
| I-1 | 27.5 | 29.6 | 20.4 | 22.9 | 31.8 | 47.7 |
| I-2 | 33.2 | 37.0 | 29.6 | 35.6 | 43.3 | 57.5 |
| II-1 | 58.7 | 63.6 | 46.8 | 52.5 | 67.8 | 79.2 |
| II-2 | 78.4 | 85.0 | 68.1 | 74.3 | 80.3 | 97.4 |

## 2.2 Model overview

This paper refers to an actual cable-stayed bridge for model establishment: bridge deck cover plate thickness 20 mm, top U rib thickness 8 mm, web thickness 60 mm, diaphragm thickness 10 mm, bottom plate thickness 16 mm, bottom U rib thickness 6 mm, wing plate thickness 30 mm, wing plate I rib thickness 16 mm, wind faring wall plate thickness 9 mm, wind faring I rib thickness 7 mm. This is shown in **Fig. 4** (a). The bridge panel is made of Q345 steel, and its dynamic mechanical properties are shown in **Table 5**.

**Table 5.** Dynamic mechanical properties of Q345 steel

| Strain rate | 0.002 | 1 | 10 | 100 | 1680 | 3040 |
|---|---|---|---|---|---|---|
| Yield strength (MPa) | 345 | 430 | 463 | 523 | 610 | 636 |
| Tensile strength (MPa) | 616 | 660 | 658 | 697 | 780 | 762 |

The main bridge is a 5-span continuous cable-stayed bridge with cable tower and steel box girder double cable plane. Its cross-border arrangement is 63 m + 257 m + 648 m + 257 m + 63 m=1288 m. It adopts a semi-floating structure system with elastic constraints in the longitudinal direction to limit the longitudinal drift of steel box girder under live load and wind load. The main beam adopts orthotropic plate flow flat steel box girder, which is 3.2 m high and 37.2 m wide (including air nozzle). It is divided into 89 beam sections, and the standard section length is 15 m. The cable is made of high strength parallel steel wire extruded with high density polyethylene (HDPE). There are 8×21 pairs in the whole bridge, and the transverse distance between the anchor points of the cable is 32.8 m. The tower is 215 m high and has four beams, among which the lower column and beam are reinforced concrete structure, and the other parts are steel structure. The height of the steel tower is 178.696 m. The section of the tower is a rectangle with four right Angle cutting angles, 5.0 m across the bridge and 6.8 m along the bridge. The main bridge substructure consists of 6 piers, with transition piers at both ends, two in the middle for the main tower foundation, and the remaining two for the auxiliary piers.

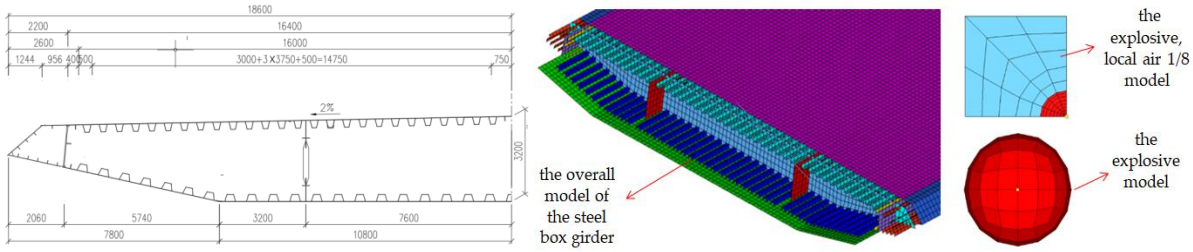


(a) 1/2 cross-sectional view (mm) (b) Finite element model of local steel box girder

**Fig. 4.** Dimensions and finite element model of bridge panel.

## 2.3 Finite element model

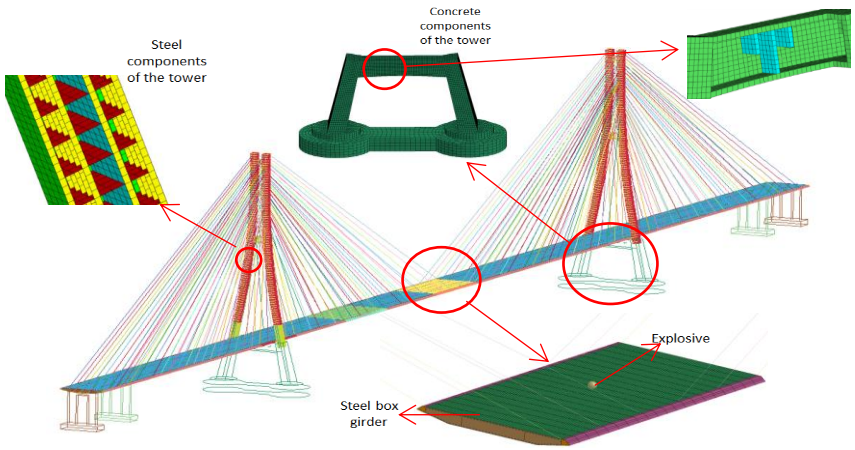


**Fig. 5.** Full bridge finite element model.

Steel box girder adopts shell element and air explosive adopts solid element. Among them, the

junction of steel box girder rib stiffeners, top plate, bottom plate, web and diaphragm are all connected by common nodes. The shape and size of the mesh of the diaphragm need to be manually controlled to meet the requirements of the quadrilateral mesh of shell elements, and there is no too large or too small angle. The shell element adopts material No. 24, and its material parameters are selected as the verification parameters in the previous two sections. The specific model is shown in **Fig. 5**. Considering the fact that the deck of cable-stayed bridge has a large axial force and cable force, it will affect the response of the deck under explosion load. In this paper, the complete restart method of LS-DYNA will be adopted. Firstly, the stable state of the whole bridge under the action of gravity is calculated. Then take out the local steel box girder and all the internal forces and deformation state of this part. Finally, the explosion load is applied for simulation.

Since the whole bridge adopts the common node mode to connect the grid cells between the internal structures, the mesh size is divided according to the transverse bridge distance between the U-shaped ribs (25-35 cm). If one cell is divided (**Fig. 6** (a)), the fracture position of the bridge panel can only be at the connection position of the U-rib and the bridge panel, and the simulation results will be unreliable. If three or more units are divided (**Fig. 6** (c)), the cost of computing time will be multiplied compared with two units, which is not conducive to the subsequent analysis of the simulation. Moreover, as can be seen from **Fig. 6** (a) and (c), the web unit cannot be common node with the top plate and bottom plate. Therefore, the unit side length of the whole bridge is controlled at about 15 cm (**Fig. 6** (b)).

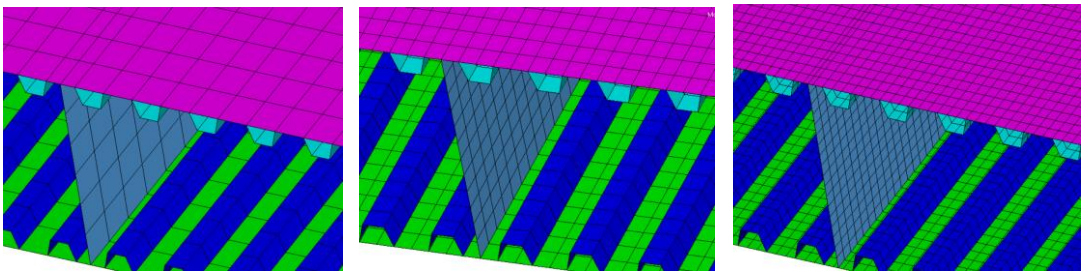

(a) About 30 cm (b) About 15 cm (c) About 10 cm

**Fig. 6.** Different mesh size models.

## 2.4 Calculation conditions

**Table 6.** Calculated working conditions (car bomb explosion on mid-span bridge deck)

| Case | Explosion Location | Equivalent (kg) | Burst Height (m) | Proportional Distance(m/ $kg^{1/3}$) |
|---|---|---|---|---|
| I-1 | 1 | 281.26 | 0.656 | 0.1 |
| I-2 | 1 | 843.78 | 0.945 | 0.1 |
| I-3 | 1 | 1898.505 | 1.238 | 0.1 |
| I-4 | 1 | 2531.34 | 1.363 | 0.1 |
| I-5 | 1 | 4500 | 1.651 | 0.1 |
| II-1 | 2 | 281.26 | 0.656 | 0.1 |
| II-2 | 2 | 843.78 | 0.945 | 0.1 |
| II-3 | 2 | 1898.505 | 1.238 | 0.1 |
| II-4 | 2 | 2531.34 | 1.363 | 0.1 |
| II-5 | 2 | 4500 | 1.651 | 0.1 |
| III-1 | 3 | 281.26 | 0.656 | 0.1 |
| III-2 | 3 | 843.78 | 0.945 | 0.1 |
| III-3 | 3 | 1898.505 | 1.238 | 0.1 |
| III-4 | 3 | 2531.34 | 1.363 | 0.1 |
| III-5 | 3 | 4500 | 1.651 | 0.1 |
| IV-1 | 4 | 281.26 | 0.656 | 0.1 |
| IV-2 | 4 | 843.78 | 0.945 | 0.1 |
| IV-3 | 4 | 1898.505 | 1.238 | 0.1 |
| IV-4 | 4 | 2531.34 | 1.363 | 0.1 |
| IV-5 | 4 | 4500 | 1.651 | 0.1 |

Consider a car bomb exploding on a mid-span bridge. In the case of car bomb explosion on the bridge deck, the proportional distance is 0.1 m/kg$^{1/3}$, and the TNT equivalent of the bomb is 200 kg~4500 kg. In America, the equivalent TNT equivalent range of car bombs is generally 200 kg-27300 kg [28, 29]. Cars that may be used as car bombs include cars, large cars, buses, vans, tank cars and trailers. Its maximum TNT equivalent (determined by maximum deadweight) is 227 kg, 455 kg, 1818 kg, 4545 kg, 13,636 kg and 27273 kg respectively [28].

The carriageway of the bridge deck is six lanes in two directions, considering that the car bomb explodes at four typical positions in the transverse bridge direction. The calculation conditions are shown in Table 6, and the charging position is shown in **Fig. 7**. The lateral positions of explosion load 1, 2, 3, and 4 are shown in **Fig. 7** (a). Explosion point 1, 3 is located above the mid-span of the cross section, and explosion point 2 is located above the web. The location of the cross bridge direction of explosion point 4 is determined according to 30 cm from the outer wheel of the vehicle to the curb stone. In the longitudinal position of the bridge (**Fig. 7** (b)), explosion points 1, 2 are located above the diaphragms, and explosion points 2, 4 are located between the two diaphragms.

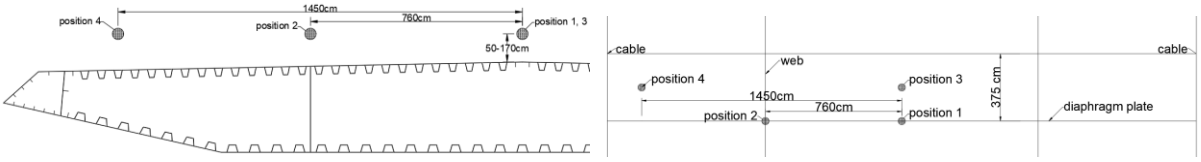


(a) Cross sectional drawing (b) Top view

**Fig. 7.** Schematic diagram of the position of the explosion sources across the bridge.

## 3 Results and discussion

In this section, the plastic deformation and energy dissipation of orthotropic steel bridge panels are studied according to the working conditions in **Table 4**, and the results of a certain working condition are taken as an example for analysis.

### 3.1 Response process of steel bridge panel

The response process is roughly divided according to plastic strain. First of all, when the bridge panel is subjected to explosion load, it will produce violent plastic deformation. At this time, the longitudinal rib stiffeners and diaphragm will play a role in constraining the deformation of the bridge panel. Secondly, the deformation is further expanded, and the longitudinal rib stiffeners also deforms violently, leading to the failure of the constraint until the deformation reaches the maximum. Finally, the dynamic steady state vibrates back and forth within a certain range of plastic deformation.

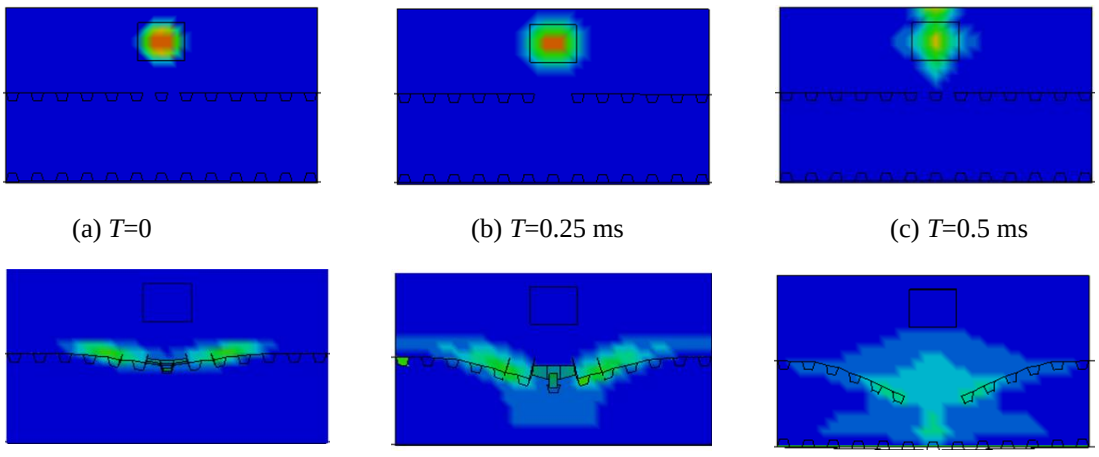

(a) $T$=0 (b) $T$=0.25 ms (c) $T$=0.5 ms

(d) $T$=1.2 ms (e) $T$=3.4 ms (f) $T$=7.2 ms

**Fig. 8.** Blast impact response of steel box girder (mid-span partial cross section, Cases I-3).

Take the simulation results of working condition I-3 as an example. It can be seen from **Fig. 8**

that when $T$<0.5 ms, the explosion wave propagates freely in the air; When $T\approx$0.5 ms, the explosion wave propagates to the roof and is reflected, and the roof begins to produce large local deformation under the action of shock wave. When $T\approx$1.2 ms, the roof breaks, and the shock wave enters the chamber and propagates downward. When $T\approx$3.4 ms, the shock wave reaches the bottom plate, interacts with the bottom plate, and the bottom plate begins to deform. At the same time, the top plate begins to produce fragments. When $T\approx$7.2 ms, the fragments reach the bottom plate and collide with the bottom plate, so that the bottom plate produces large plastic deformation, but the bottom plate is not cracked. At the same time, after the top plate is broken, the cover plate tears along the stiffening rib to produce petals and crimping. When $T\approx$30 ms, the steel box girder tends to be stable and the response is basically over.

### 3.2 The deformation mode

According to the analysis of all working conditions, the response process of failure mode of steel box girder can be divided into three types:

Type I, the cover plate and the rib stiffeners act together. The cover plate is not damaged, only deformation occurs, and the rib stiffeners do not break, which plays a supporting role on the bridge panel.

Type II, the cover plate and the rib stiffeners are detached, the cover plate is damaged, only the bridge panel is partially cracked, other members are not cracked.

Type III, disengagement of the cover plate from the rib stiffeners, extensive failure of the cover plate, fracture of the rib stiffeners with no support constraints to the bridge panel, and cracking of the bottom plate or web.

### 3.3 Deformation and energy dissipation

**Fig. 9** shows the kinetic energy and deformation energy time-history curves of I-type steel bridge panel under I-1 working condition. In the figure, the total energy is the energy input to the bridge panel by the explosion impact, which is equal to the initial kinetic energy of the bridge panel. It can be seen from **Fig. 9** (a) that the energy exerted by the explosion impact on the steel bridge panel is mainly absorbed and dissipated by the plastic deformation of the bridge panel. At about 0.01 s, most of the kinetic energy of the steel bridge panel is transformed into deformation energy dissipation. It can be seen from **Fig. 9** (b) that during the deformation development of the bridge panel, because the deformation of the cover plate is limited by the rib stiffeners and diaphragms, the rib stiffeners and diaphragms obtain certain kinetic energy, which is partially or completely transformed into the plastic deformation energy dissipation of the rib stiffeners and diaphragms. In **Fig. 9** (b), the deformation energy consumption of the cover plate, the longitudinal rib stiffeners and the diaphragm account for 40.3%, 31.3% and 21.4% of the total energy respectively. In addition, the unit fails due to the longitudinal rib stiffeners breaking away from the cover plate, resulting in a certain calculation loss (about 4.0% of the total energy).

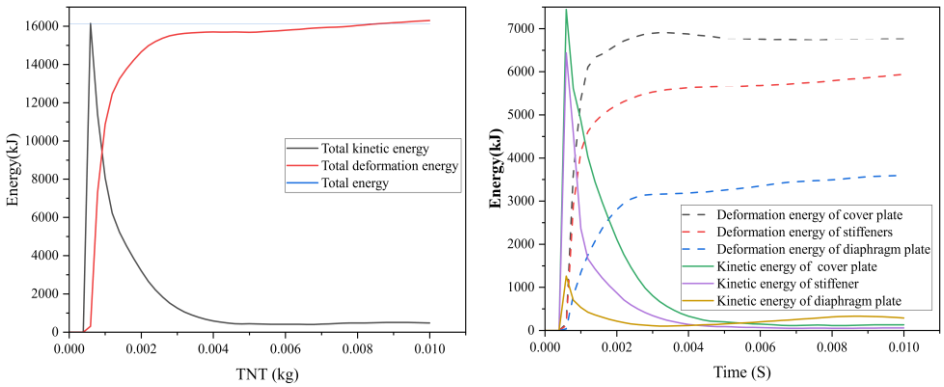


**Fig. 9.** Time-history curves of deformation energy dissipation and kinetic energy of steel bridge Panel (Cases I-1 of Type I).

### 3.4 Crevasse process

**Fig. 10** shows the breach formation process of bridge deck under the explosion of 4500 kg TNT equivalent. It can be seen that when $T$<1.0 ms, it is a typical local deformation (no cracking) of the plate, and the plate deformation is significantly larger than that of the longitudinal stiffened plate and the diaphragm. When 1.0 ms <$T$<1.2 ms, the single element plastic strain at the connection between the cover plate and the longitudinal rib stiffeners first reach the threshold to form a crack, and the crack expands along the direction of the rib stiffeners. When $T$=1.6 ms, the center area of the cover plate forms a fragment of about 0.88 m in length and 0.4 m in width, and the center area of the longitudinal stiffening rib forms a fragment of about 1 m in length. When $T$>1.6 ms, under the action of residual kinetic energy, the cover plate is torn and curled backward to form petals. When 1.6 ms<$T$<3.4 ms, the transverse petals are constrained by the longitudinal rib stiffeners, forming plastic hinges near the joints. At $T$=3.4 ms , the shock wave reaches the bottom plate and deforms it. When $T$>3.4 ms, the petals rotate around the plastic hinges until they reach an equilibrium position. The longitudinal rib stiffeners are constrained by the diaphragm in the back bending process, and finally shows a vertical downward curling shape. And at $T$=7.2 ms, the fragment collides with the bottom plate.

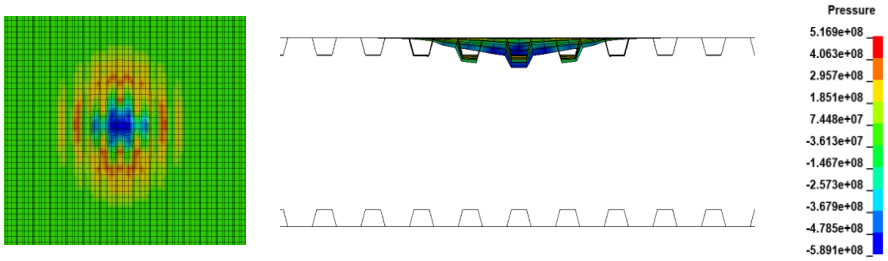


(**a**) T=1.0 ms

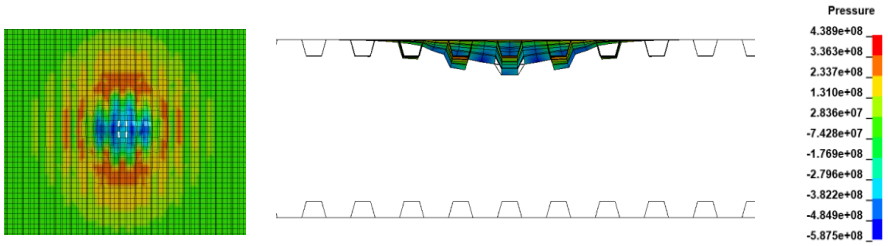


(**b**) T=1.2 ms

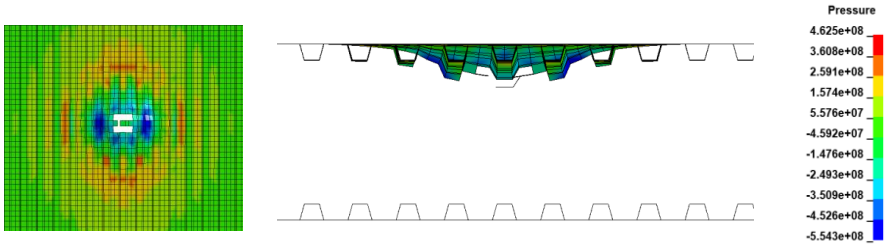


(c) T=1.6 ms

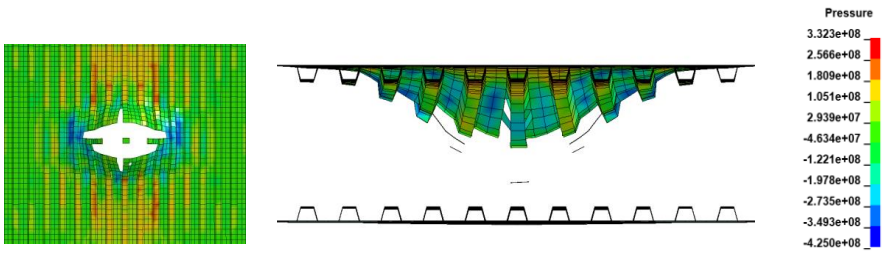


(d) T=3.4 ms

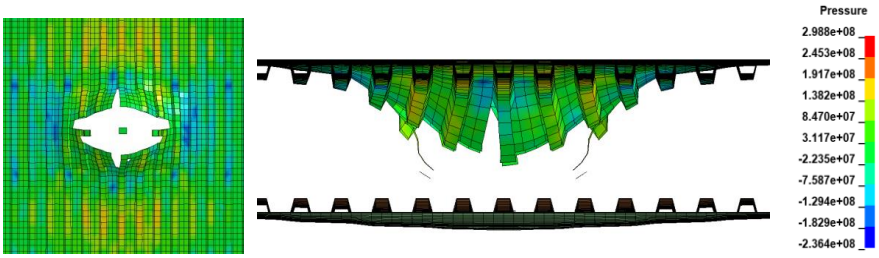


(e) T=7.2 ms

**Fig. 10.** Fracture formation process of steel bridge panel (Unit: N ).

In conclusion, the process of bridge panel breach can be divided into three stages: The first stage is the bridge panel breach stage. When the shock wave reaches the bridge panel, the bridge panel rapidly undergoes local large deformation, and then cracks and breaks, producing fragments, forming petals and curling. The second stage is the action stage of shock wave on the diaphragm and bottom plate. The shock wave propagates inside the box body and is used for the bulkhead, web and bottom plate. The third stage is the impact of fragments on the bottom plate. The bridge panel fragments hit the bottom plate at high speed, resulting in large plastic deformation.

### 3.5 Deformation energy dissipation and fragmentation kinetic energy

**Fig. 11** shows the energy time history curve of the steel bridge panel under the explosion impact of 4500 kg TNT. Where: the total energy is the explosion impact input energy, the total energy dissipation is the sum of the total deformation energy and the total kinetic energy, the total deformation energy includes the deformation energy of the cover plate, the diaphragm and the rib stiffeners, the total kinetic energy includes the kinetic energy of the cover plate and the longitudinal rib stiffeners. The steel bridge panel cracks and breaks under the impact of explosion, and the calculated energy loss caused by the deletion of a large number of units in the calculation is equal to the total energy (input energy) minus the total energy consumption excluding the calculated loss. Two cases of the total deformation energy including the calculated loss and without the calculated loss are given in the figure. The energy without calculation loss can be extracted directly by software shortcut function; The element is deleted because its deformation is too large, so the energy loss generated by calculation is approximately added to the total deformation energy consumption, and the deformation energy consumption including calculation loss is obtained.

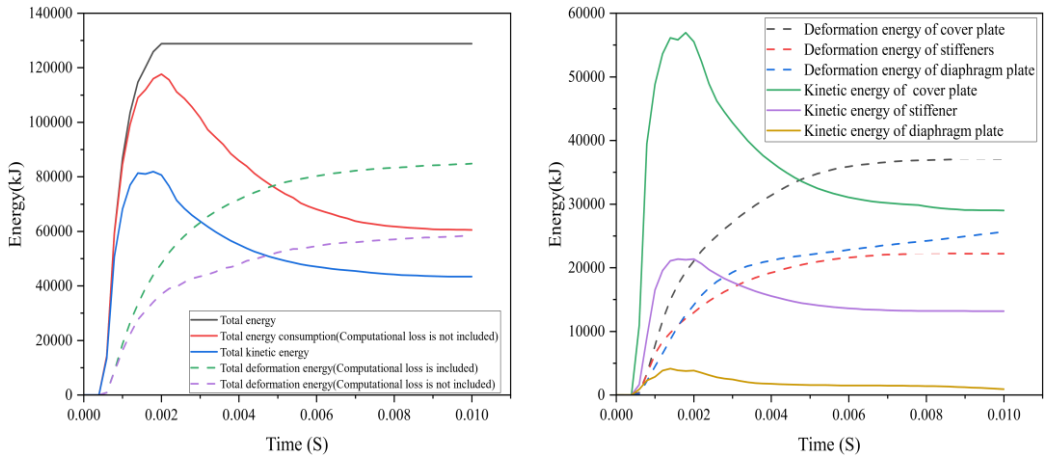


(a) Time history curve of total energy change

(b) Time history of energy change of each component (including calculation loss)

**Fig. 11.** Energy time history curve of steel bridge panel (4500 kg, I-5).

According to **Fig. 11** (a), the kinetic energy of the fragment and the total deformation energy dissipation account for about 10% and 90% of the total energy, respectively, when the calculation loss is included. Without calculation loss, the total energy consumption decreases with the action time and becomes stable at about 0.09 s. The total kinetic energy of the bridge panel does not decay to zero, and the remaining kinetic energy is the

fragment kinetic energy. It can be seen from **Fig. 11** (b) that at about 0.01 s, the deformation energy dissipation of the cover plate, the diaphragm plate and the rib stiffeners all reach a stable value, and the remaining kinetic energy of the cover plate and the rib stiffeners is the fragment kinetic energy.

Based on the results of working conditions I-1~I-5, the energy consumption ratio of each component of the steel bridge panel under the explosion of 281 kg~4500 kg TNT equivalent is summarized, as shown in Table 5.

In **Table 7** and **Fig. 12**, the curves of explosion input energy and various energy absorption of steel bridge panels as a function of charge amount are presented when TNT is 281 kg~4500 kg. In **Fig. 12** (a), (b), the total deformation energy consumption is included in the calculated energy loss caused by the deletion of the unit; In figure 12 (c), the total deformation energy consumption, the deformation energy consumption of the cover plate and the longitudinal rib stiffeners are not included in the calculation loss.

**Table 7.** Energy consumption ratio of each component of steel bridge panel under different TNT equivalent explosive.

| TNT equivalent (kg) | Blast impact energy input (kJ) | Energy consumption in total energy (%) | | | | | |
|---|---|---|---|---|---|---|---|
| | | Deformation energy consumption (not counting energy loss) | | | | Total fragment kinetic energy | Calculation loss |
| | | Cover plate | Stiffening rib | Diaphragm plate | Deformation energy dissipation | | |
| 281.26 | 16780 | 40.34 | 31.28 | 21.41 | 93.03 | 2.96 | 4.01 |
| 843.78 | 31760 | 37.76 | 28.68 | 20.24 | 86.68 | 4.34 | 8.98 |
| 1898.51 | 59812 | 32.92 | 23.80 | 18.04 | 74.76 | 12.44 | 12.8 |
| 2531.34 | 76642 | 30.02 | 20.87 | 16.72 | 67.61 | 17.34 | 15.05 |
| 4500 | 128850 | 20.98 | 11.77 | 12.60 | 45.35 | 32.51 | 22.14 |

It can be seen from **Fig. 12** that the explosion input energy, total deformation energy consumption (including calculation loss) and fragment kinetic energy of the steel bridge panel all increase with the increase of charging amount, and the proportion of fragment kinetic energy in the input energy gradually increases, but the proportion of total deformation energy consumption in the input energy gradually decreases. The larger the loading amount, the more failure units of the calculation model of steel bridge panel, the greater the energy loss. When the charging amount is relatively small, with the increase of the charging amount, the plastic deformation energy consumption ratio of the cover plate increases, while the plastic deformation energy consumption ratio of the longitudinal rib stiffeners rib and the diaphragm plate decreases. When the loading amount is large, with the increase of loading amount, the plastic deformation energy consumption ratio of the cover plate and the longitudinal rib stiffeners decreases gradually, while the plastic deformation range of the diaphragm increases, and the plastic deformation energy consumption ratio also increases.

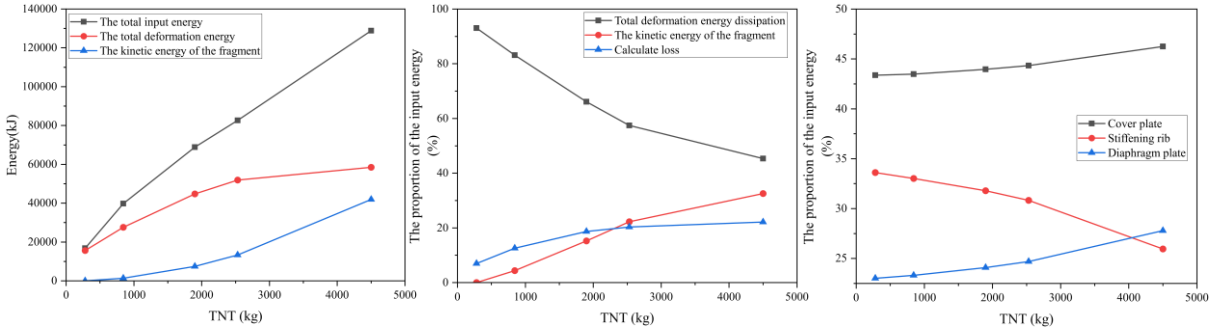


(a) Energy consumption distribution

(b) The proportion of each energy dissipation to the total energy

(c) Energy dissipation allocation for deformation (excluding calculated loss)

**Fig. 12.** Energy dissipation curve of steel bridge panel.

### 3.6 Energy dissipation distribution at different explosion locations

As can be seen from **Fig. 7**, position 2 is directly above the web, so under the action of explosion load, it will also play a certain constraint role on the bridge panel. By comparing the energy

distribution at position 1-3, the main anti-explosion structures of the bridge structure under the action of bridge deck explosion can be obtained.

**Fig. 12** shows the energy distribution diagram of working condition II-5 and III-5, including the energy loss. By comparing **Fig. 13** (a) and **Fig. 11** (b), it can be seen that the energy dissipation capacity of the web is second only to that of the bridge panel, and the maximum kinetic energy of the bridge panel is reduced, and the damage range is reduced. Compared with **Fig. 13** (b), although the explosion position is between the diaphragm, the shock wave reaches the inside of the box beam and is used to deform the diaphragm to achieve the purpose of energy consumption. Therefore, the web and diaphragm plate play a relatively large role in supporting the bridge panel.

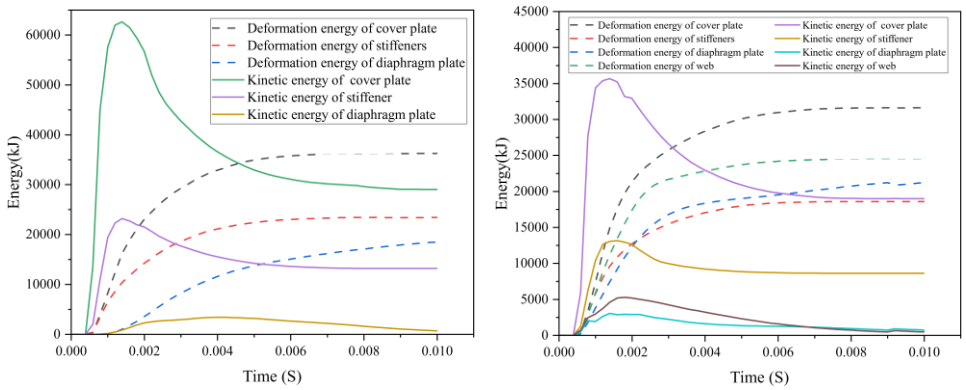


(a) Case II-5 (b) Case III-5

**Fig. 13.** Time history of energy change of each component (including calculation loss; 4500 kg).

### 3.7 Response of stay cables to explosion

The dynamic relaxation in LS-DYNA is used to simulate the pre-tension tension of the stay cable. The specific operation is to carry out the dynamic relaxation of the whole bridge to make the whole bridge stable. The cable force of each cable is taken as the initial condition of the dynamic relaxation of the next cable model. The reference standard is that the mid-span deflection is negligible relative to the length of the main span as far as possible under the action of static load, and the calculation time cost is taken into account, so we choose to cycle twice.

Position 4 is set near the stay cable, as shown in **Fig. 7**. According to the design specification, the minimum distance between the outermost wheel of the vehicle and the stone along the road is 0.5 m to determine the lateral distribution position of the explosion [30]. According to the distance from the cable, the longitudinal distribution location of the explosion is determined.

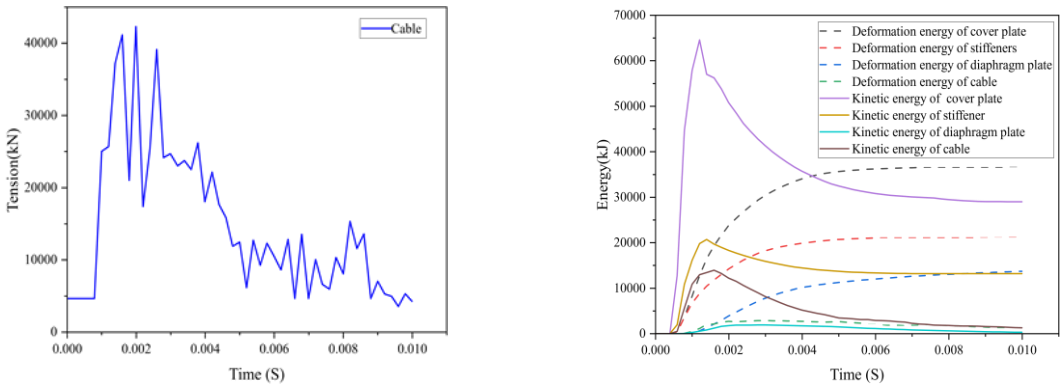


(a) Time history curve of cable force

(b) Time history of energy change of each component (including calculation loss)

**Fig. 14.** Time history curve of case III-5.

According to **Fig. 14** (a), the force of the cable under the action of explosion load reaches about

eight times of the normal value, which is four times of the maximum bearing capacity of the cable. Therefore, the cable will break under the explosion load, which will affect the stability of the whole bridge. In addition, the unit in the anchorage position was also damaged, indicating that the cable may be pulled out from inside the box girder during the response process, leading to cable failure. According to **Fig. 14** (b), the kinetic energy and deformation energy of the cable are very low, indicating that they play little role in anti-knock performance. However, the stay cable is very important for the stability of the whole bridge, and it is easy to be damaged, so the protection and reinforcement of the stay cable is particularly important.

## 4 Conclusion

This study investigates the plastic deformation, fracture and energy distribution of orthotropic steel bridge panel under the impact of car bomb explosions. The reasonable computing models of orthotropic steel bridge panel of steel box girder are determined. The plastic deformation, energy dissipation, cracking and damage process of steel box girders in different cases are studied and comparatively analyzed. The following conclusions can be drawn.

(1) The failure mode of orthotropic steel bridge panel under blast impact is mainly local damage. For the steel box girder in this paper, the longitudinal bridge dimension of bridge panel calculation model can be 10 m, with simple supports at both ends.

(2) If the TNT equivalent is less than 280 kilograms, the cover plate will not crack and the bridge panel will appear local plastic deformation. With the increase of loading amount, the bridge panel shows three failure modes: mode 1, the longitudinal rib stiffeners do not break away from the cover plate, and the cover plate, longitudinal rib stiffeners and diaphragm coordinate deformation; In mode 2, the longitudinal rib stiffeners are removed from the cover plate, but not cracked; Mode 3, longitudinal rib stiffeners disengage and break.

(3) The cracks and breaks will occur on the bridge panel when the TNT equivalent of the explosive is large than 840 kilograms. When the explosive yield exceeds 1,900 kilograms, the bridge panels can cause serious damage. The damage process can be divided into three stages: local plate deformation, fragment formation and petal formation.

(4) For bridge deck explosion, the main energy dissipation components of steel girders are the bridge panel, web, diaphragm and rib stiffeners. When the explosion shock wave acts on the steel girder, the explosion will generate high temperature, which will greatly weaken the strength of steel, causing further damage.

(5) As one of the most important components of the cable-stayed bridge, attention should be paid to the damage of the cable, which will affect the whole bridge. In serious cases, P-Δ effect (i.e., gravity secondary effect) may occur, which will lead to the continuous collapse of the whole bridge.

(6) Although this paper only analyzes the bridge deck of a specific size, due to the local damage caused by the explosion load, and the purpose of this paper is to analyze the key energy-consuming components of the bridge panel under the action of the explosion load, the analysis results can be divided into two categories: One is the transverse mid-span position, where all the structure of the bridge panel is symmetrically stressed, which can be simulated as the response of each component of a large bridge under the action of explosion load. The other is the lateral edge, where the force on the bridge panel is asymmetrical, which can be simulated as the response of each component of a small bridge under the action of explosion load.

**Funding:** This research was funded by the National Natural Science Foundation of China (Grant No. 52278188), the Natural Science Foundation of Jiangsu Province (Grant No. BK20211196), and the “Six-Talent Peaks” Project of Jiangsu Province (Grant No. 2019-JZ-013).

**Conflicts of Interest:** The authors declare no conflict of interest.

## References

[1] NCHRP. Blast-resistant highway bridges-design and detailing guidelines (report 645). Transportation Research Board 2010.
[2] Mozos CM, Aparicio AC. Parametric study on the dynamic response of cable stayed bridges to the sudden failure of a stay, Part I: bending moment acting on the deck. Engineering Structures 2010; 32(10): 3288-3300. https://doi.org/10.1016/j.engstruct.2010.07.002
[3] Bigs JM. Introduction to structure dynamics. McGraw-Hill, New York, the United States, 1964.
[4] Ni ZH. Vibration Mechanics. Xi 'an Jiaotong University Press, Xi 'an, China, 1994.
[5] Zhu CM; Zhang WP. Structural Mechanics. Higher Education Press, Beijing, China, 2009.
[6] AASHTO. AASHTO LRFD bridge design specifications. Washington, D.C.: American Association of State Highway and Transportation Officials, 2007.
[7] Mozos CM, Aparicio AC. Parametric study on the dynamic response of cable stayed bridges to the sudden failure of a stay, Part II: bending moment acting on the pylons and stress on the stays. Engineering Structures 2010; 32(10): 3301-3312. https://doi.org/10.1016/j.engstruct.2010.07.002
[8] Zhou Y, Chen S. Numerical investigation of cable breakage events on long-span cable-stayed bridges under stochastic traffic and wind. Engineering Structures 2015; 105: 299-315. https://doi.org/10.1016/j. engstruct.2015.07. 009
[9] Hashemi SK, Bradford MA, Valipour HR. Dynamic response and performance of cable-stayed bridges under blast load: Effects of pylon geometry. Engineering Structures 2017; 137: 55-66. https://doi.org/ 10.1016/j.engstruct.2017.01.032
[10] Mazurkiewicz L, Malachowski J, Baranowski P. Blast loading influence on load carrying capacity of I-column. Engineering Structures 2015; 104: 107-115. https://doi.org/10.1016/j.engstruct.2015.09.025
[11] Elsa G, Cristina T. Analysis of the mass and deformation variation rates over time and their influence on long-term durability for specimens of porous material. Sustainable Structures 2022; 2(1): 000014. https: //doi.org 10.54113/j.sust.2022.000014
[12] Sun YX, Wang X. Damage effect of steel circular tube subjected to fire and blast. Journal of Constructional Steel Research 2021; 176: 106389. https://doi.org/10.1016/j.jcsr.2020.106389
[13] Song KJ, Long Y, Ji C, et al. Experimental and numerical studies on the deformation and tearing of X70 pipelines subjected to localized blast loading. Thin-Walled Structures 2016; 107: 156-168. https://doi.org /10.1016/j. tws.2016.03.010
[14] Williams G D, Williamson E B. Procedure for predicting blast loads acting on bridge columns. Journal of Bridge Engineering 2012; 17(3): 490-499. 9. https://doi.org/10.1061/(asce)be.1943-5592.0000265
[15] Zhang YY, Pan RY, Dias-da-Costa Daniel. An energy-based method for assessing the equivalent static force of a vehicle collision with bridge columns. Structure and Infrastructure Engineering 2022; 18(8): 1107-1119. https://doi. org/10.1080/15732479.2021.1895228
[16] Zhu C, Ma RJ, Chen AR. Damage Characteristics of Steel Girder and RC Pylon of Cable-supported Bridge Suffered from Blast Loading. Journal of Highway and Transportation Research and Development 2016; 33(8):92-98. https://doi. org/10.3969 /j.issn.1002-0268.2016.08.014
[17] Ibrahim A, Salim H. Numerical prediction of the dynamic response of prestressed concrete box girder bridges under blast loads. 11th International LS-DYNA Users Conference, 2006.
[18] Wei XY, Bai GL. Dynamic response and failure pattern analysis of reinforced concrete column under explosion load. Journal of PLA University of Science and Technology (Natural Science Edition) 2007; 05:55-529.
[19] Shi YC. Dynamic response behavior and damage mechanism of reinforced concrete structures under explosion load. Tianjin University, 2009.
[20] Yao SJ. Numerical simulation of local failure of steel box girder internal explosion. National University of Defense Technology, 2012.
[21] Yu JH. Study on the effect and protection of bridge pier under underwater explosion load. Wuhan University of Technology, 2014.
[22] Deng RB, Jin XL, et al. Numerical Simulation of Damage Effect of Bridge under Explosion Shock Wave. Journal of Shanghai jiaotong university 2008; 42 (11): 1927-1930. 9. https://doi. org/10.16183/j.carol carroll nki jsjtu. 2008.11.039

[23] Tang EKC, Hao H. Numerical simulation of a cable-stayed bridge response to blast loads, Part I: Model development and response calculations. Engineering Structures 2010; 32 (10): 3180-3192. https://doi.org/10.1016/j. engstruct.2010.06.007

[24] Wang Y. Vertical bending response of suspension bridge under air Explosion Shock wave. National University of Defense Technology, 2010.

[25] Chen HY, Zeng XG, et al. Under explosion loading bridge dynamic response and damage process of numerical simulation. Journal of sichuan university 2011; 06:15-19. https://doi.org/10.15961/j.j suese.2011.06.001

[26] Xing Y. Study on Explosion Failure Mechanism and Safety Assessment Method of Urban Bridge. Tianjin University, 2014.

[27] Zhao N, Yao SJ, et al. Experimental and numerical studies on the dynamic response of stiffened plates under confined blast loads. Thin-Walled Structures2020; 154: 106839. https://doi.org/10.1016/j.tws.2020.106839

[28] B. Ham D, Lockwood S. National Needs Assessment for Ensuring Transportation Infrastructure Security. Vienna: AASHTO Transportation Security Task Force, 2002.

[29] Wu J, Liu JB, Du YX. Elastic-plastic Dynamic Calculation and Numerical Analysis of prefabricated Explosion-proof Wall under Car Bomb Explosion. Journal of Disaster Prevention and Mitigation 2007; 27(4): 394-399. https://doi.org/10.113409/j.cnki.jdpme.2007.04.001

[30] Ministry of Transport, PRC. General Specifications for Design of Highway Bridges and Culverts. People's Communications Publishing House, Beijing, China, D60-2015.